J Mater Sci (2008) 43:3806–3811
DOI 10.1007/s10853-007-2303-5

Local strain analysis in twin boundaries in ultrafine grained copper

Mohamed Sennour · Sylvie Lartigue-Korinek · Yannick Champion · Martin J. Hÿtch

Received: 16 August 2007 / Accepted: 8 November 2007 / Published online: 13 March 2008

Abstract Elastic properties of grain boundaries (GBs) influence the macroscopic behavior of materials such as their resistance to deformation but have proved extremely difficult to measure experimentally. Conventional techniques for studying elastic properties of materials can only provide a macroscopic (grains + boundaries) average response. In this work, local strain measurements using geometric phase analysis have been carried out in ultrafine grained copper (UFG) on twin boundaries containing dislocations. Experimental results and simulations using isotropic elasticity reveal an easier deformability of the boundary compared to the matrix. Enrichment of the boundaries in dislocations during deformation seems to eliminate this effect by mutual canceling of the strain fields from adjacent dislocations.

Introduction

Grain boundaries (GBs) play a major role in the mechanical behavior of materials such as strengthening and fracture resistance [1], and affect several other properties such as diffusion [2], slip transmission [3], and grain boundary sliding [4, 5]. Consequently, GBs have been a subject of intense research in order to investigate their structure and properties. In this respect, elastic properties of GBs have proved extremely difficult to measure experimentally since the many techniques developed to study elastic properties of materials can only provide a macroscopic average response of grains and boundaries. The measurements carried out on bicrystals have been rare and limited to yield and fracture stresses [6]. However, it is often assumed that GBs are elastically weaker than the bulk ideal crystal. Indeed, atomistic calculations [7, 8] and indirect experimental evidence [9] emphasize that some elastic moduli may be much less at grain boundaries than that in the crystalline matrix. This has been used to explain the decrease of the Young modulus with decreasing grain size in nanocrystalline materials where GBs volume fraction is important [10, 11].

In the present work, GBs elastic properties are investigated using a totally different approach. This is based on the accurate determination of local strains at GBs from HRTEM images by Geometric Phase Analysis (GPA) [12]. GPA has been used previously for the analysis of dislocations [13], low-angle grain boundaries [14], and twin boundaries [15]. The latter case is similar to that treated in this article. The approach uses a dislocation as a probe to apply localized stresses to a grain boundary and simultaneously measure the elastic response. For more details about the approach and arguments of its validity the reader can refer to this article.

Investigations are carried out on coherent $\Sigma 3(111)$ twin boundaries (CTBs) in ultrafine grained copper. An extensive analysis of twin structure and defects has been performed on this material [16], which has been shown to combine ultrahigh strength and ductility [17]. Processes for the decomposition of dislocations in twin boundaries have been discussed, with grain boundaries acting as sources and sinks for dislocations. After mechanical deformation, there is an enrichment of twins in dislocations. Their

M. Sennour · S. Lartigue-Korinek (✉) · Y. Champion
Institut de Chimie et Matériaux Paris Est, UMR CNRS 7182, CECM, 94407 Vitry sur Seine, France
e-mail: sylvie.lartigue@glvt-cnrs.fr

M. J. Hÿtch
CEMES-CNRS, 29 rue J. Marvig, 31055 Toulouse, France

arrangement as quasi-periodic arrays reveals that diffusional processes are active at room temperature, in contrast to coarse-grained copper [16]. From a deformation behavior point of view, coherent twins form a rather rigid element of the microstructure; they have a low energy and low diffusivity and can be used to probe postmortem grain boundary/dislocations interactions.

A recent study carried out on germanium using the GPA technique revealed that the incorporation of dislocations into a Σ3(111) coherent boundary softens it by up to 50% [15]. Thus, it will be interesting to determine whether this is a specific characteristic of germanium or rather a general property of twin boundaries in metals. Furthermore, results will provide valuable information on "mechanical" behavior of nanocrystalline materials' twin boundaries.

Experimental procedures

Bulk UFG copper specimens are produced through powder metallurgy processing of nanocrystalline powders [18]. For HRTEM observations, thin foils are mechanically polished to ~100 μm of thickness followed by an electrochemical thinning at −15 °C in order to limit oxidation of the samples. Images are acquired using a TOPCON 002B microscope operating at 200 kV (Cs:0.4 mm, point resolution: 0.185 nm) and the negatives digitized at 0.0366 nm per pixel. Image analysis was carried out using in-house routines written for Digital Micrograph 3.5 (Gatan). Image distortions due to the microscope aberrations, notably those due to the projector lenses, have been calibrated on silicon single crystal and eliminated from the HREM images before analysis [19]. In addition, images presented in the article have been Fourier-filtered to eliminate noise. The masks used in Fourier space for this filtering are of the same size as that used in the geometric phase analysis. Lattice fringes were analyzed by applying Gaussian masks in reciprocal space of radius 0.8 nm^{-1} producing a lateral resolution in the phase images of 1.25 nm.

Results

Figure 1a shows an HRTEM image obtained on a Σ3(111) ⟨110⟩ twin boundary (TB) and where atomic columns are white. TB presents a particular faceted form with long coherent {111} facets connected by short incoherent {112} segments. The latter have been identified as having a 9R structure. Careful inspection of the image highlights the presence of a dislocation at the junction of the {111} and {112} facets. Circuit mapping [20] around the steps showed that most defects present a Burgers vector of the type $\mathbf{b} = \frac{1}{3}[\bar{1}\bar{1}1]_1 = \frac{1}{3}[\bar{1}\bar{1}\bar{1}]_2$ (Fig. 1b). Some steps are associated with perfect dislocations $\frac{1}{2}[110]_1$ (lower step on

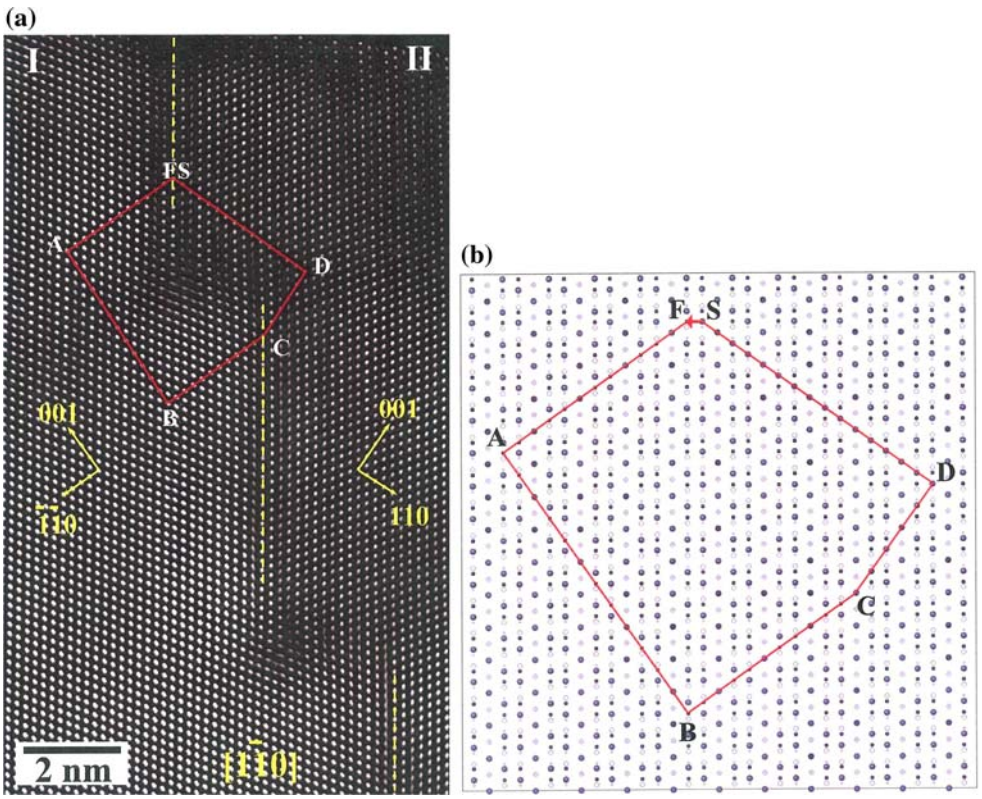

Fig. 1 (**a**) HRTEM image obtained along $[1\bar{1}0]$ zone axis on a faceted twin boundary in the as-processed specimen showing a supplementary (111) plane located at the {111}/{112} junctions; Circuit around the higher step reported in the dichromatic complex (**b**): $FS = \mathbf{b} = \frac{1}{3}[\bar{1}\bar{1}1]_1 = \frac{1}{3}[\bar{1}\bar{1}\bar{1}]_2$. The site C is common to both crystals. Small circles correspond to atoms in crystal 1, large circles to atoms in crystal 2. (Filled circles: $z = 0$, empty circles: $z = 0.5$)

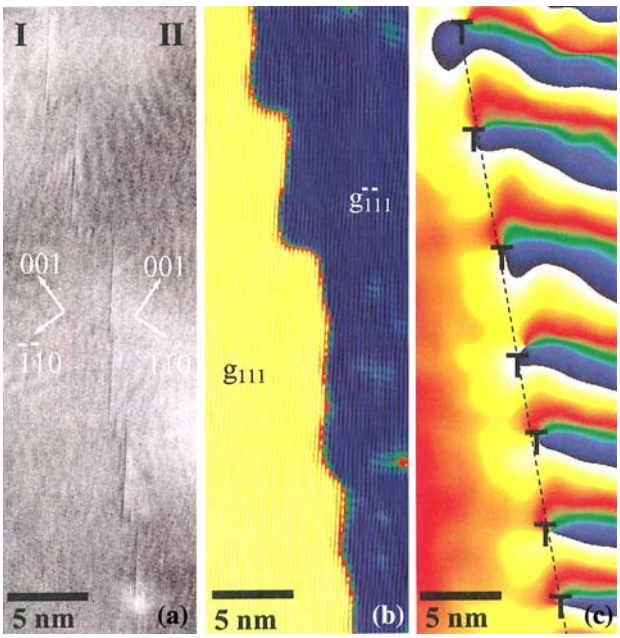

Fig. 2 (**a**) HRTEM image of the whole faceted Σ3(111) ⟨110⟩ twin boundary; (**b**) Phase image calculated from $\mathbf{g}_1 = (111)_1$ and $\mathbf{g}_2 = (\bar{1}\bar{1}1)_2$ corresponding to both twinned crystals 1 and 2; (**c**) Phase image obtained from the common $(11\bar{1})_1$ and $(111)_2$ fringes. Discontinuities correspond to intergranular dislocations core. (For color see online version)

Fig. 1). As shown below from GPA analysis, these dislocations are decomposed into a Frank dislocation and a dislocation with $\mathbf{b} = \frac{1}{6}[\bar{1}\bar{1}\bar{2}]$. Glissile dislocations with $\mathbf{b} = \frac{1}{6}\langle 112\rangle$ are also encountered along the coherent parts of the twins.

GPA has been carried out on the whole twin boundary (Fig. 2a). The geometric phase images are obtained by applying two masks on $\mathbf{g}_1 = (111)_1$ and $\mathbf{g}_2 = (\bar{1}\bar{1}1)_2$ (1 and 2 denotes both twinned crystals) allowing a clear visualization of the faceted morphology of the boundary (Fig. 2b). Figure 2c shows the phase image calculated from the common {111} fringes by applying a Gaussian mask around the $\mathbf{g}_1' = (11\bar{1})_1$ and $\mathbf{g}_2' = (111)_2$ reflections. Discontinuities on the image correspond to dislocation cores [13]. It is worth noting that even sessile dislocations are principally localized on {111}/{112} junctions. They are aligned and regularly spaced. This indicates that they have been able to reorganize themselves as a quasi-periodic array in order to accommodate the deviation from the perfect twin orientation.

Measurement of the displacement perpendicular to the twin boundary, u_x, is straightforward as the {111} planes are parallel on either side of the boundary. However, measurement of displacement parallel to the boundary, u_y, is more problematic as the other set of {111} fringes are not parallel in both crystals, due to the twin. Displacements are therefore measured separately in grain 1 and grain 2 using references: $\mathbf{g}_1 = (111)_1$, $\mathbf{g}_1' = (11\bar{1})_1$, $\mathbf{g}_2 = (\bar{1}\bar{1}1)_2$, $\mathbf{g}_2' = (111)_2$ (more details are given in reference [15]).

Strains, ε_{ij}, and local rigid-body rotations, ω_{ij}, were then computed by differentiating the displacement field in each crystal:

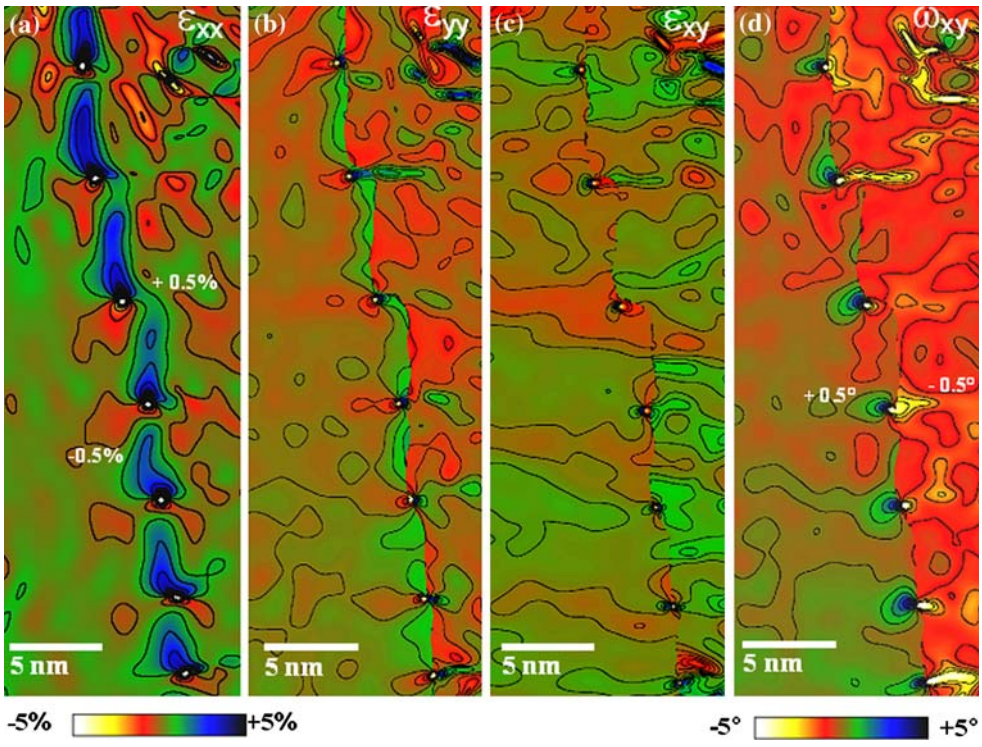

Fig. 3 Local strains measured experimentally using GPA from HRTEM image of Fig. 2**a**: (**a**) ε_{xx} strain (inset image indicates expansion and contraction region around dislocation core); (**b**) ε_{yy} strain; (**c**) ε_{xy} shear strain; (**d**) ω_{xy} local rotation map. Contours every 0.5% from −2.5% to +2.5% strain and every 0.5° from −2.5° to +2.5° rotation. (For color see online version)

$$\varepsilon_{ij} = \frac{1}{2}\left(\frac{\partial u_i}{\partial x_j} + \frac{\partial u_j}{\partial x_i}\right) \quad (1)$$

$$\omega_{ij} = \frac{1}{2}\left(\frac{\partial u_j}{\partial x_i} - \frac{\partial u_i}{\partial x_j}\right) \quad (2)$$

and the results are combined (Fig. 3a–d).

Strains are concentrated around the dislocation cores, which are highly localized. In regions below the dislocation cores, lattice planes are in compression to accommodate the extra half-plane. They are in expansion above the defect. However, when analyzing the strain distribution, the most interesting feature is the ε_{xx} strain localization along the coherent boundary (Fig. 3a). Indeed, the regions in expansion above the dislocation cores display strongly extended strains localized along the boundary plane: there is a clear increase of expansion (maximum of 1.5% with respect to the nondeformed matrix) over several atomic planes on both sides of the boundary. However, below the dislocations, strains are distributed "symmetrically" around dislocation cores and no strain localization is observed. In fact, as the expansion part is along the twin plane and the supplementary plane is in the crystal, the elastic response on the upper part and the lower part of the dislocation is expected to be different. Comparison with what was observed in the case of germanium [15], where the expansion and the contraction parts are along the boundary, confirms that TBs behave differently owing to the presence of a large step in the present twins.

The strain component, ε_{yy}, parallel to the boundary and the shear component, ε_{xy}, are continuous across the boundary and no localized strains are visible. Slight discontinuity at the twin is probably due to artifacts from image analysis: the piece-wise calculation of the strains, absent from ε_{xx} due to the common lattice planes parallel to the boundary, and the derivatives at the boundary plane where lattice fringes contrast goes to zero induce artificial strains observed particularly for ε_{xy} [15].

The lattice rotation map derived from the phase image via Eq. 2 is shown in Fig. 3d. The highest rotations are localized around the dislocation cores themselves. Between dislocations, the orientation varies smoothly from one grain to the other one across the boundary. The lobes are mainly extended parallel to $[11\bar{1}]_1 = [111]_2$, which is in agreement with Burgers vector (BV) of the type $\mathbf{b} = \frac{1}{3}[\bar{1}\bar{1}1]_1 = \frac{1}{3}[\bar{1}\bar{1}\bar{1}]_2$ [17]. The measured deviation from the prefect twin orientation (1.5°) agrees perfectly with the deviation calculated from this distribution, showing that the Frank dislocations mainly accommodate the deviation.

After a 40% compression test, twin boundaries are enriched in dislocations and the boundary structure is more complex (Fig. 4). HRTEM images reveal a significant decrease of step heights compared to the as-processed specimen. No offset of the extra plane in the neighboring grain is now observed. Using circuit mapping analysis, dislocations have also been identified as sessile Frank dislocations with Burgers vectors (BVs) of the type $\mathbf{b} = \frac{1}{3}[\bar{1}\bar{1}1]_1 = \frac{1}{3}[\bar{1}\bar{1}\bar{1}]_2$ (note lobe orientation parallel to $[11\bar{1}]_1 = [111]_2$ in (Fig. 5c).

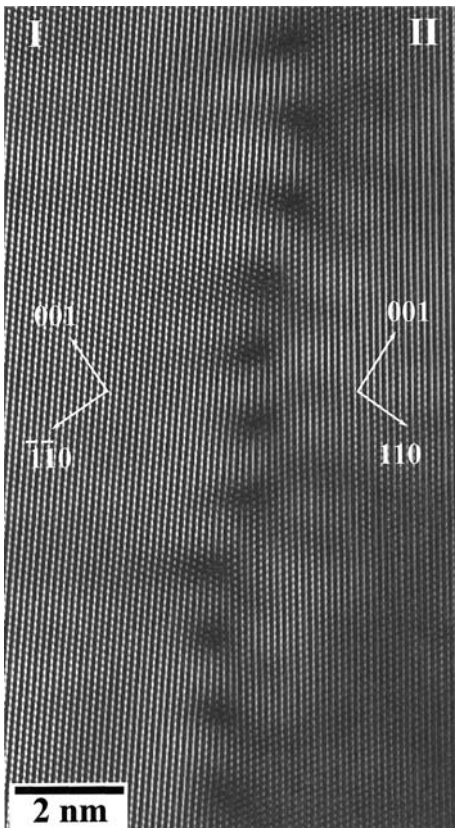

Fig. 4 HRTEM image obtained along $[1\bar{1}0]$ zone axis of a Σ3(111) ⟨110⟩ twin boundary in the deformed specimen

The complexity of TBs structure in the deformed specimen does not allow a similar analysis as for the as-processed material. Nevertheless, the fact that (111) is parallel on either side of the boundary allowed calculation of local rotation (ω_{xy}) and strain (ε_{xx}) maps (Fig. 5a, c). The good agreement between the experimental and the calculated dislocation spacing, 2.35 nm and 2.39 nm, respectively, clearly indicates the accommodation of the deviation from the perfect twin orientation ($\Delta\theta = 5°$) by dislocation reorganization. This requires short-range diffusion along the interface and might be supplemented by pipe-diffusion. On the other hand, the strain distribution and local rotation of the dislocation array of Fig. 4 simulated using isotropic elasticity shows a good agreement with the experimental image (Fig. 5b, d).

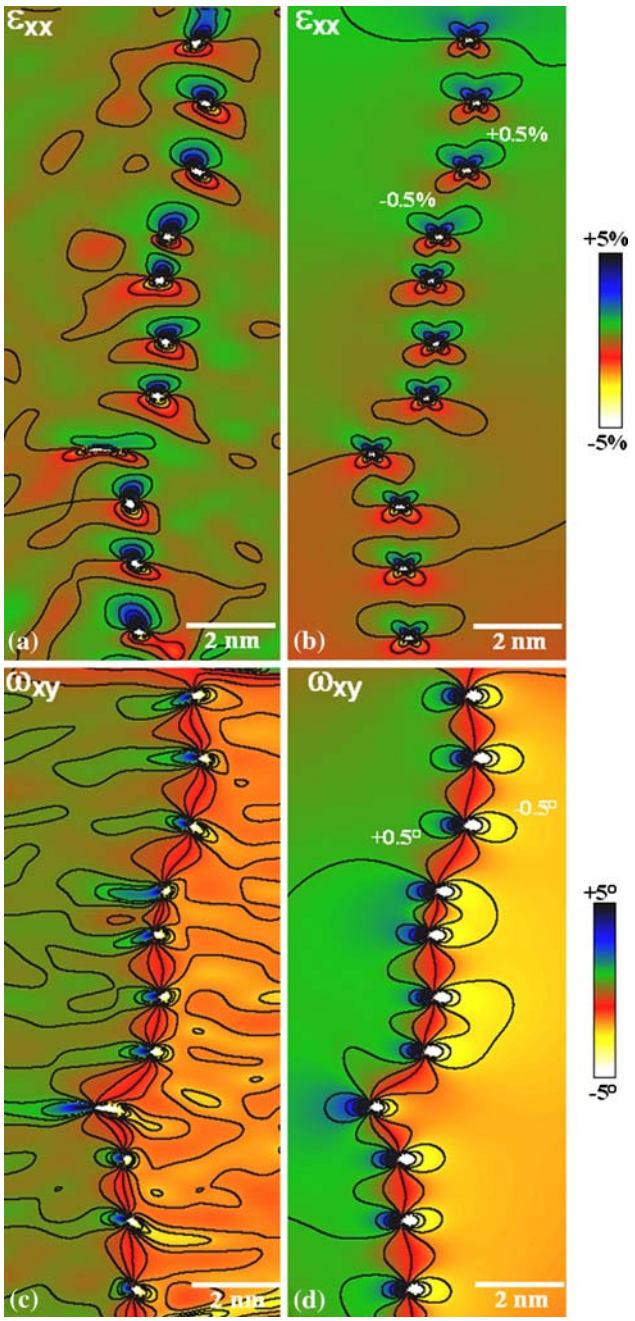

Fig. 5 Local strains and rotation measured experimentally and calculated using GPA (isotropic elasticity) from HRTEM image of Fig. 4: (**a**) and (**b**) experimental and simulated ε_{xx} strain respectively, (**b**) and (**d**) experimental and simulated local rotation ω_{xy} respectively. Contours every 0.5% from −2.5% to + 2.5% strain and every 0.5° from −2.5° to +2.5° rotation. (For color see online version)

The most interesting feature is the absence of ε_{xx} strain localization along the boundary (Fig. 5a). Indeed, after deformation, strains are mainly localized around dislocation cores and no strain extension is observed either in the expansion or contraction region of dislocations. This is unlike the as-processed specimen and requires discussion.

Discussion

Using GPA, twin boundary defects in ultrafine grained copper have been investigated. GPA has been previously applied in the case of a constricted 60° dislocation in TB in Germanium [15]. The particularity of the present study is the fact that TBs have a specific form with long coherent facets (111) planes and small incoherent facets ((112) planes), sessile Frank dislocations being localized at the facets junction. Moreover, the relatively small dislocation spacing, especially in the case of the deformed specimen, is interesting as interactions between dislocations influence the distribution of strain fields.

Strains at TBs in the as-processed specimen are localized around the dislocation cores except for the component of the deformation perpendicular to the boundary, ε_{xx}, which extends along the coherent boundary. It appears that this strain field extension is characteristic of the twin boundary effect. Indeed, the extension is not observed for contracted regions of the lattice since these are localized inside grains, and not at the TB, due to faceting (Fig. 3).

Furthermore, it is instructive to compare these results with the case of a lattice dislocation in the absence of a grain boundary. Figure 6a and b shows the ε_{xx} strain and local rotation ω_{xy} maps obtained for an isolated lattice dislocation and the corresponding simulated maps using isotropic elastic theory (Fig. 6c, d). As it can be observed,

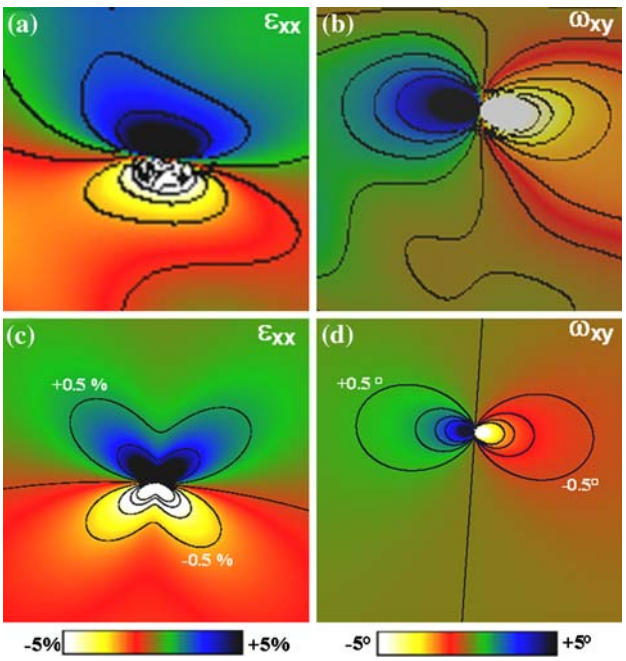

Fig. 6 ε_{xx} strain and ω_{xy} local rotation of an isolated Frank dislocation (**a** and **b**) and the corresponding isotropic elastic simulation (**c** and **d**). Contours every 0.5% from −2% to +2% strain and every 0.5° from −2° to +2° rotation. (For color see online version)

the main experimental features are well-reproduced including lobe shapes and orientation. However, no strain extension is observed.

It is extremely unlikely that the expansion and contraction measured across the boundary plane could be due to imaging artifacts or to rigid-body displacements induced by structural changes in the twin boundary. Indeed, analysis of TBs free of dislocations does not reveal any strain localization along the boundary.

Coherent twin boundaries are expected to be the stiffest of grain boundaries; nevertheless, they can be considered as more deformable than the matrix. In germanium, the incorporation of a dislocation into a Σ3(111) coherent boundary softened it by up to 50% [15]. A similar effect is observed in the case of intrinsic Frank type grain boundary dislocations arranged in a quasi-periodic array.

The absence of strain extension in the case of the deformed specimen is worth noting. All the more, the steps are very small (1–2 atomic planes) so that both expansion and contraction regions, above and below dislocation cores, are localized on the boundary plane. This would lead to strain localization above and below dislocation cores as observed in germanium.

On the other hand, the resolution of the GPA method is related to the size of the mask used for calculating the phase image. In our case, lattice fringes were analyzed by applying Gaussian masks in reciprocal space of radius 0.8 nm^{-1} producing a lateral resolution in the phase images of 1.25 nm. Hence, the latter might be attributed to the fact that dislocations are closer to each other than for the as-processed specimen. Indeed, dislocations enrichment of TBs during deformation diminishes significantly the dislocation spacing. This was highlighted experimentally: the mean value of dislocation array periodicity is 2.35 nm for the deformed specimen compared to 6.5 nm in the case of the as-processed specimen [16]. Consequently, lattice plane expansions above a dislocation core are compensated by the contraction of lattice planes under the adjacent dislocation core.

From the mechanical behavior point of view of ultrafine grained copper, accommodation processes of dislocations occur at GBs during deformation at room temperature, as witnessed from the dislocation arrangement at twin boundaries.

Conclusion

Twin boundaries in ultrafine grained copper have been analyzed using high-resolution microscopy and geometric phase analysis. TBs are in majority faceted into coherent {111} and incoherent {112} facets with a Frank dislocation lying at the junction of the facets.

Measurements of local strains revealed an extension along the boundary of the dislocation strain field (ε_{xx}) corresponding to lattice displacement perpendicular to the TB. Comparison with isotropic elastic theory in the case of an isolated dislocation confirmed that such an effect is characteristic of the twin boundary. This is interpreted as an "easier" deformability of twin boundary compared to the matrix. The absence of strain localization along TB in the case of deformed (40%) specimen has been attributed to TB enrichment in dislocations during deformation causing mutual annulment of expansion and contraction effects between close adjacent dislocations.

References

1. Sutton AP, Balluffi RW (1995) Interfaces in crystalline materials. Clarendon Press, Oxford
2. Peterson NL (1983) Int Met Rev 28:65
3. Clark WAT, Wagoner RH, Shen ZY, Lee TC, Robertson IM, Birnbaum HK (1992) Scripta Metall 26:203
4. Ashby AH (1972) Surf Sci 31:498
5. Watanabe T (1983) Metall Trans A 14:531
6. Su JQ, Demura M, Hirano T (2003) Acta Mater 51:2505
7. Kluge MD, Wolf D, Lutsko JF, Phillpot SR (1990) J Appl Phys 67:2370
8. Alber I, Bassani JL, Khanta M, Vitek V, Wang GJ (1992) Phil Trans Roy Soc London A 339:555
9. Xu T, Zheng L (2004) Phil Mag Lett 84:225
10. Kim HS, Bush MB (1999) Nanostruct Mater 11:361
11. Haque MA, Saif MTA (2004) PNAS 1001:6335
12. Hÿtch MJ, Snoeck E, Kilaas R (1998) Ultramicroscopy 74:131
13. Hÿtch MJ, Putaux JL, Penisson JM (2003) Nature 423:270
14. Johnson CL, Hÿtch MJ, Buseck PR (2004) PNAS 101:17936
15. Hÿtch MJ, Putaux J-L, Thibault J (2006) Phil Mag 86:4641
16. Sennour M, Lartigue-Korinek S, Champion Y, Hÿtch MJ (2007) Phil Mag 87:1465
17. Champion Y, Langlois C, Guérin-Mailly S, Langlois P, Bonnetien J-L, Hytch MJ (2003) Science 300:310
18. Langlois C, Hÿtch MJ, Langlois P, Lartigue-Korinek S, Champion Y (2005) Metall Mater Trans A 36A:3451
19. Hüe F, Johnson CL, Lartigue Korinek S, Hytch M (2005) J Elect Microsc 54(3):181
20. Pond RC, Hirth JP (1994) Solid State Phys 47:288